Nonlinear tolerancing through high fidelity variation simulation of deformable parts under frictional contact

Citation for the original published paper (version of record):
Sadeghi Tabar, R., Wärmefjord, K., Lindkvist, L. et al (2026). Nonlinear tolerancing through high fidelity variation simulation of deformable parts under
frictional contact. CIRP Annals - Manufacturing Technology, 75(1): 155-159.
http://dx.doi.org/10.1016/j.cirp.2026.04.084

(article starts on next page)

CIRP Annals - Manufacturing Technology 75 (2026) 155–159

Contents lists available at ScienceDirect

CIRP Annals - Manufacturing Technology

journal homepage: https://www.editorialmanager.com/CIRP/default.aspx

Nonlinear tolerancing through high fidelity variation simulation of deformable parts under frictional contact

Roham Sadeghi Tabar*, Kristina Wärmefjord, Lars Lindkvist, Rikard Söderberg (1)

Chalmers University of Technology, Department of Industrial and Materials Science, SE 412-96 Gothenburg, Sweden

A R T I C L E I N F O

Article history:
Available online 1 May 2026

Keywords:
Tolerancing
Friction
Quality assurance

A B S T R A C T

Friction at contact interface strongly influences deformable assembly variation, yet most nonrigid variation simulation tolerancing workflows still assume frictionless contact. This paper presents a novel nonlinear variation simulation and unilateral contact considering Coulomb friction solved as a second order cone program, enabling nonlinear tolerancing with practical computational cost. The method is demonstrated on an industrial assembly with perturbed geometries. Compared to a frictionless baseline, the proposed model captures stick and slip effects and yields lower tangential slip and reduced variation across defined contact zones. The results highlight the necessity of frictional contact modeling for tolerance analysis in assemblies.

1. Introduction

Geometric variation in sheet metal assemblies originates from part and process deviations and propagates through manufacturing and joining operations. Geometry assurance methods address this across product development stages. Early stages typically apply statistical variation analysis on preliminary CAD to assess sensitivity and robustness, and tolerance cost [1,2]. Later stages employ FEM based, deformable assembly models to capture deformation and springback during clamping and joining [3,4]. These methods enable prediction and control of variation prior to physical builds. Industry trends now leverage individualized assembly [3] and Digital Twins [5] to close the loop between specification, simulation, and inline or offline metrology, optimizing part matching [6], locator settings, and joining and clamping sequences in near real time [3,7,8]. Despite this progress, friction at contact interfaces between components, governing stick or slip, and local compliance during positioning, clamping, and joining has been underrepresented in variation simulation and tolerancing models. Incorporating realistic frictional contact behavior improves predictive fidelity of assembly outcomes. Recent studies have proposed efficient approaches for including contact effects in deformable variation analysis [7,9]. This paper examines how friction coupling alters interface forces, contact areas, and resulting geometric variation by integrating frictional effects into tolerance analysis for geometry assurance of deformable assemblies.

1.1. Tolerancing in deformable assemblies

Tolerancing research spans tolerance definition, allocation, analysis, and evaluation across product development stages [10].

For rigid assemblies, tolerance analysis is typically performed using worst case or statistical methods, often implemented in computer aided tolerancing (CAT) tools to propagate dimensional and geometric variation through assembly models [3]. However, for deformable assemblies, geometric outcomes depend not only on part deviations but also on assembly parameters, i.e., locating scheme, clamping and joining strategy [11,12]. Contact interactions govern load transfer and constraint enforcement, and even small disturbances in the locating scheme may produce large geometric deviations [9]. Consequently, accurate prediction of assembly behavior becomes critical for robust fixture design and sequence optimization [13].

1.2. Statistical variation simulation for deformable assemblies

Statistical tolerancing represents assembly behavior under uncertainty by assuming probabilistic distributions for part deviations and estimating the assembly response through repeated sampling [14]. Monte Carlo (MC) simulation is particularly common in CAT environments for rigid body variation analysis, and has recently been integrated with admissible limits [15]. In deformable assemblies, interface behavior strongly influences the final geometry because contact interactions govern load transfer and constraint enforcement. Traditional CAT workflows often rely on nominal CAD geometry and simplified contact assumptions, which is insufficient when local interface mechanics dominate the assembly response. Skin model shapes provide a more realistic representation of manufactured geometry at interfaces [16–18]. Building on this, the present work focuses on the contact interface as the primary carrier of variation. Crucially, we extend the linear tolerance analysis through the method of influence coefficients (MIC) [12], to include nonlinear contact behavior arising from Coulomb friction. Friction introduces tangential constraints and stick slip transitions that modify how loads are transmitted through the assembly and, consequently, how geometric

* Corresponding author.
E-mail address: rohams@chalmers.se (R. Sadeghi Tabar).

https://doi.org/10.1016/j.cirp.2026.04.084

variation accumulates locally and globally. In this work, we therefore compute frictional contact displacements and systematically compare them to a frictionless baseline. The outcome is a contact level variation behavior, i.e., normal and tangential displacement components per contact, which are directly attributable to the interface mechanics.

1.3. Scope of the paper

Traditional tolerance analysis approaches for deformable sheet metals assumes a linear relationship between part and assembly variation, which oversimplifies assembly physics. The contact interfaces governed by unilateral normal contact and the tangential frictional behavior play a critical role in determining geometric variation. This paper proposes a nonlinear tolerancing approach addressing the frictional contact behavior verified using force measurement data and a comparison with a baseline frictionless approach.

2. Proposed nonlinear tolerancing approach

The MIC provides an efficient reduced order alternative to repeated full FEM assembly solves in nonrigid variation simulation (NRVS). The underlying FE models employ linear shell elements with six degrees of freedom (DOF) per node. Parts are modeled as linear elastic bodies under small deformations and quasi static loading. Geometric deviations, locator, and clamp offsets are introduced as initial misfits as gaps or overclosures at interfaces [12]. Contact constraints with unilateral normal contact determine which interfaces are in active contact and what interface forces are developed [9]. The resulting contact forces are mapped to displacements through precomputed influence coefficients. Here, a new 3D MIC is introduced to capture the tangential displacement at each sampled geometry. The overview of this approach is presented in Fig. 1.

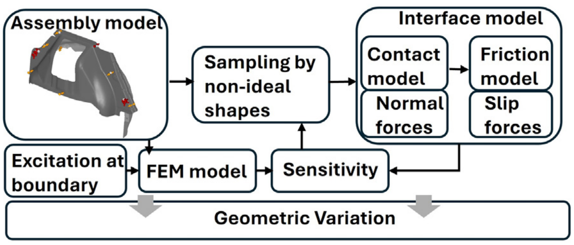

Fig. 1. Overview of the proposed nonlinear NRVS approach.

Consider part p with FE displacement vector u_p and stiffness matrix $\boldsymbol{K}_p$. Under linear elasticity:

$$\boldsymbol{K}_p u_p = f_p. \tag{1}$$

Let the DOFs be partitioned into boundary conditions, clamps and locator nodes, and their associated DOFs, and the remaining internal DOFs. With the standard FE partitioning, eliminating the retained interface DOFs yields a reduced relation at the interface:

$$u_i = \boldsymbol{H}_p f_c + u_i(0), \tag{2}$$

where $\boldsymbol{H}_p$ is the contact compliance matrix, f_c contact forces, and $u_i^{(0)}$ denotes any known displacement contribution from boundary conditions. The influence coefficients, the entries of $\boldsymbol{H}_p$, represent the displacement at an interface DOF due to a unit load applied at another interface DOF. In practice, $\boldsymbol{H}_p$ is obtained by factorizing $\boldsymbol{K}_p$ once and solving multiple right hand sides associated with interface unit loads.

2.1. Contact model

In NRVS, contact modeling is essential to prevent virtual penetration between mating surfaces and to accurately predict assembly deformation and springback. Contact forces arising at interfaces influence part positioning, clamping, and joining, making them critical for realistic simulation. Assuming m candidate contact pairs indexed by $k = 1, \ldots, m$, for each contact pair k, a local orthonormal frame (n_k, t_{1k}, t_{2k}) at the nominal contact point is defined, assembled in the 3×3 orthonormal matrix $\boldsymbol{R}_k = [n_k, t_{1k}, t_{2k}]$, which maps global displacements to the local normal and tangential coordinate system. Let u_i stack all interface DOFs of all parts in global coordinates. The linear operator $\boldsymbol{G}_k$ maps the global interface DOFs to the relative displacement, $\delta_k{}^g$, at the contact pair k in global coordinates, and is defined as:

$$\delta_k{}^g = \boldsymbol{G}_k u_i \in R^3. \tag{3}$$

To transform to local coordinates, the following is considered:

$$\delta_k = \boldsymbol{R}_k{}^T \delta_k{}^g = \left[\delta_{n,k}, \delta_{t1,k}, \delta_{t2,k}\right]^T. \tag{4}$$

Geometric deviations, locator errors, and manufacturing shape errors are introduced through an initial deviation $g_k{}^{(0)}$ in the same local coordinate system. With the normal gap convention $g_{n,k} > 0$ denoting separation, the normal gap is:

$$g_{n,k} = g_{n,k}{}^{(0)} + \delta_{n,k}. \tag{5}$$

Contact modeling also accounts for joining operations, e.g., spot welds [13] and springback, requiring two contact resolution steps per MC iteration. Automatic contact detection through KD tree search [19] is performed to identify contacting areas on the nominal geometry. Thermal influences have been incorporated into the method for higher fidelity [19]. Despite the increased complexity, incorporating frictional effects and prior enhancements enables integration with digital twin frameworks [3,7], supporting real time geometry assurance in production.

Let $f_k = \left[f_{n,k}, f_{t1,k}, f_{t2,k}\right]^T$ be the discrete contact force resultants at contact pair k in the local frame, and stack all contact forces in $f \in R^{(3m)}$. Contact forces act on the interface DOFs through an assembly distribution operator $\boldsymbol{C}$ that applies equal and opposite forces to the paired nodes and accounts for the local to global transformation:

$$f_i = \boldsymbol{C}^T f. \tag{6}$$

Using the assembled interface compliance $\boldsymbol{H}$ and the condensed relation $u_i = \boldsymbol{H} f_i + u_i{}^{(0)}$, the stacked relative displacements at all contact pairs in local coordinates can be written as:

$$\delta = \delta^{(0)} + \boldsymbol{S} f, \tag{7}$$

where $\boldsymbol{S}$ is the assembly 3D influence matrix. The matrix $\boldsymbol{S}$ is the core reduced operator. It maps contact forces directly to induced relative motions, normal and tangential, at all candidate contacts. The normal gap vector is then:

$$g_n = g_n{}^{(0)} + \delta_n{}^{(0)} + \boldsymbol{S}_{nn} f_n + \boldsymbol{S}_{nt} f_t, \tag{8}$$

with $\boldsymbol{S}$ partitioned into normal, $\boldsymbol{S}_{nn}$, and tangential blocks, $\boldsymbol{S}_{nt}$ in the local frames. In frictionless contact, only the normal block is used. For each contact k, frictionless unilateral contact is given by:

$$g_{n,k} \geq 0,\ f_{n,k} \geq 0,\ g_{n,k} f_{n,k} = 0. \tag{9}$$

These conditions enforce nonpenetration, compressive only normal forces, and complementarity. Therefore, either the contact is open ($g_{n,k} > 0, f_{n,k} = 0$) or closed ($g_{n,k} = 0, f_{n,k} \geq 0$).

2.2. Friction model

With a tangential force vector $f_{t,k}$ = ($f_{t1,k}$, $f_{t2,k}$) and the Coulomb friction coefficient, μ_k, the friction cone is defined as:

$$\| f_{t,k} \|_2 \leq \mu_k f_{n,k},\ f_{n,k} \geq 0. \tag{10}$$

Stick and slip are characterized by whether the inequality is a strict stick or an active slip. In slip, $f_{t,k}$ lies on the cone boundary and opposes the tangential relative motion direction. In reduced formulations, friction is commonly enforced through second order cone constraints combined with an active set strategy for open or closed contacts and stick or slip states. The computational form is obtained by solving directly for the contact force vector f using the influence matrix $\boldsymbol{S}$. Let $b = g^{(0)} + \delta^{(0)}$ denote the stacked initial deviation and free relative motions in local coordinates. A standard reduced complementary energy objective is:

$$\min_{f} \ \frac{1}{2} f^T \boldsymbol{S} f + b^T f, \tag{11}$$

subject to the admissibility constraints implied by contact and friction. For frictionless contact, only normal forces $f_n \in R^m$ are unknown, leading to the convex quadratic program (QP):

$$\min_{f_n} \ \frac{1}{2} f_n{}^T \boldsymbol{S}_{nn} f_n + b_n{}^T f_n, \ s.t. \ b_n + \boldsymbol{S}_{nn} f_n \geq 0, \ f_n \geq 0. \tag{12}$$

Here, the first constraint is the nonpenetration condition for the positive forces.

With Coulomb friction, the reduced problem can be written as:

$$\min_{f} \ \frac{1}{2} f^T \boldsymbol{S} f + b^T f, \ s.t. \ b_n + \boldsymbol{S}_{nn} f_n + \boldsymbol{S}_{nt} f_t \geq 0, \tag{13}$$

$$f_{n,k} \geq 0, \ \| f_{t,k} \|_2 \leq \mu_k f_{n,k} \ \text{ for } k = 1, \ldots, m.$$

The second order cone constraint enforce Coulomb friction, while the linear constraints ensure nonpenetration. This convex formulation can be solved using interior point second order cone program (SOCP) solvers, offering polynomial complexity and robust convergence even for large scale deformable assemblies.

2.3. Nonrigid variation simulation steps

NRVS is commonly performed in process steps, i.e., locating, joining, releasing from fixture and springback, in which new constraints and potential contacts are activated. For a given step z, the initial deviation b_z is updated based on part deviations, locator offsets, and the current assembly state. The influence matrix $\boldsymbol{S}_z$ is then assembled for the active interface, and the reduced contact problem is solved for f_z. The interface displacements are recovered as $u_{i,z} = u_{i,z}^{(0)} + \boldsymbol{HC}^T f_z$, and key characteristics at measurement points are computed via additional influence operators. Finally, the updated assembly state is propagated to the subsequent step. With this proposed frictional NRVS approach, the expensive FE solve is converted into the precomputation of compliance operators, enabling rapid repeated evaluations for sensitivity analysis, sampling, and closed loop optimization in digital twins. Friction modeling is critical in overconstrained and highly deformable assemblies where local compliance, and friction driven stick slip determine final part position and springback.

3. Case study

3.1. Reference assembly

To verify and validate the proposed method and assess its performance, this study investigates the assembly of the wheelhouse of a passenger vehicle consisting of two steel sheet components joined by five weld points. Both parts have a thickness of 0.7 mm and a material stiffness of 210 GPa. The assembly includes five weld points and 102 contact points, with each part positioned in the fixture using an 8-2-1 locating scheme. Fig. 2 illustrates the assembly model, where weld points and locating elements are indicated by spheres and filled arrows, respectively.

A batch of 500 nonideal input geometries with deformed meshes introduces variation into the frictional contact analysis. These deviations serve as input to the friction model, which accounts for normal direction contact behavior. To replicate geometric errors, corrective forces are applied at six designated points. Three contact zones (CZ), 1–3 highlighted in Fig. 2, are discretized into 102 contact points. The friction coefficient is set to μ = 0.27 for an effective steel friction level consistent with fixture clamp contact conditions. The contact problem is solved after the parts are positioned and clamped in the fixture, and the resulting forces and displacements are analyzed near the clamps in each CZ to identify potential slip under the clamps.

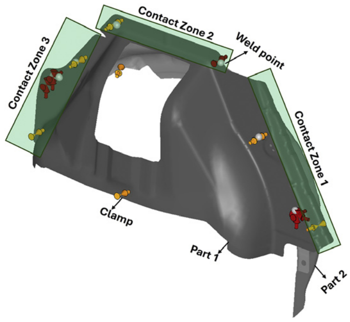

Fig. 2. The reference assembly held in the inspection fixture and welded.

3.2. Experimental measurement data

In [20] slip forces were experimentally measured to establish a reference for evaluating slip effects due to clamp forces. A stack of feeler gauges, each with a nominal plate thickness of 0.1 mm, was clamped against the finger block. A dynamometer was connected to the gauges, and a manual force was applied to determine the maximum force required before slippage occurred. Measurements were conducted on twelve different clamp and finger block configurations within the fixture. Although the measurement procedure introduces variability, the experiments provide order of magnitude estimates of slip force levels relevant for fixture contact behavior. For each locator, the measured slip force values in Newton (N) were summarized by their sample mean μ and sample standard deviation σ. A Gaussian density shape $N(\mu, \sigma^2)$ was then plotted centered at the locator position in Fig. 3. These measurements serve as the baseline for comparing slip force with simulation results.

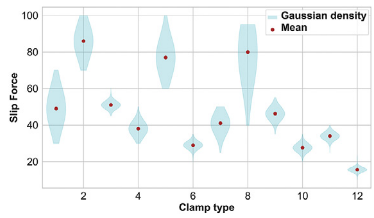

Fig. 3. The slip force (N) measurements for different clamp types.

4. Results and discussion

The proposed nonlinear tolerancing approach considering frictional contact has been developed and successfully applied to the reference assembly. The case study, therefore, serves both as a demonstration and a verification of the proposed frictional tolerancing formulation. For variation simulation, 500 input samples, Section 3, have been evaluated. To derive the sensitivity matrices, the CAT tool RD&T [21] with an in built FEM solver has been utilized. The formulations (12), and (13) are solved with OSQP and ECOS solvers in Python CVXPY, respectively.

4.1. Evaluation metrics and validation

To validate the results, the force measurements presented in Fig. 3 are compared with the calculated slip forces in the assembly at all contact points. After confirming that the predicted slip forces fall within the experimentally observed range, the Root Mean Squared (RMS) of the tangential displacement resulting from frictional forces for the contacts in each CZ is captured and compared with the unilateral frictionless contact conditions. At each CZ, the mean and 6σ of the slip displacements are compared for the 500 input samples.

4.2. Slip force and displacement predictions

The slip forces are calculated for the 102 contact points and the 500 input samples, and the mean and 6σ of the forces are reported at each contact in Fig. 4. The measured slip force mean, and variation

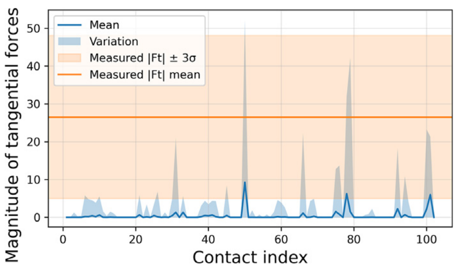

Fig. 4. Slip force variation calculated at contact versus measured surface to surface slip force (unit in N).

for the concentrated clamp types 6, 10 and 12 are presented to compare to the calculated forces. The measured slip forces span from 5 N to 48 N with a mean of 28 N. The calculated friction force variation at active contact points is 1 N to 51 N.

The experimental measurements provide order of magnitude estimates of slip forces under fixture conditions. The predicted force magnitudes fall within the measured range and reproduce the observed order of magnitude and spatial trends across contact locations. Furthermore, the forces in the normal direction, f_n and the orthogonal tangential directions, f_{t1} and f_{t2}, are analyzed, for frictional and frictionless cases, at each contact for one sample input, in Fig. 5. This is to provide a detailed force comparison at each contact. It is observed that the normal direction forces, f_n, are well aligned in both cases in active contacts. For the active contacts, the tangential couplings also modify the normal forces to be smaller in scale. This comparison has also been performed on the displacement field, u_n, u_{t1} and u_{t2} in Fig. 6. Here, it is observed that tangential displacements are smaller in scale in the frictional case as compared to the frictionless one. This is also expected since the tangential forces in the frictionless case are zero, and therefore, there are no resisting forces, and this causes the u_{t1} and u_{t2} to be larger in scale.

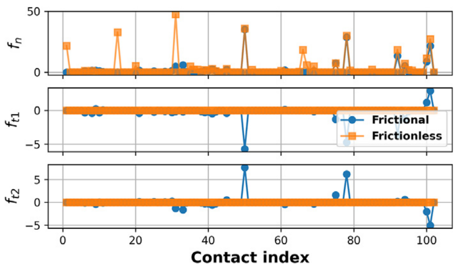

Fig. 5. Calculated forces at contact points (unit in N).

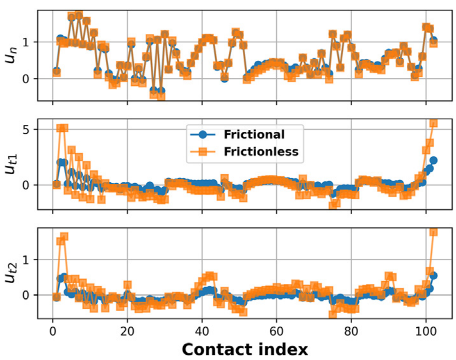

Fig. 6. Calculated displacements at contact points (unit in mm).

Table 1 presents the mean and variation 6σ of RMS of the slip displacements over the three CZs for the 500 sample inputs. This applies to both frictionless NRVS and frictional NRVS. This is accompanied by Fig. 7, where the probability densities of the RMS of contact slip displacement of the three CZs are presented. Here, it is observed that in CZ 1, not only is there a mean shift between the frictional and frictionless NRVS, but also the variation has been dampened in the frictional case. A similar behavior can be seen in the other two zones,

Table 1
RMS of Slip displacements over the contact zones (CZ) for 500 input samples (units in mm).

	Frictionless NRVS		Frictional NRVS	
Zones	Mean	Variation (6σ)	Mean	Variation (6σ)
CZ 1	0.9582	0.2940	0.4083	0.1254
CZ 2	0.8459	0.2668	0.4225	0.1167
CZ 3	1.9592	0.5944	0.8107	0.2529

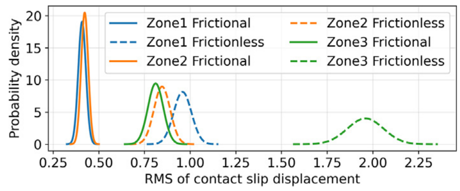

Fig. 7. Gaussian process distribution of the slip displacements over the three contact zones (units in mm).

where there is a mean shift towards reduced slip displacements in frictional NRVS, and the variation has been dampened. In CZ 3, the mean shift is more considerable, with a value of −1.14 mm and a variation reduction of 0.34 mm. Due to the presence of multiple clamps and locators locking the tangential displacements, it is expected that frictional slip is smaller compared to the free frictionless NRVS.

5. Conclusion

This paper presented a novel nonlinear tolerancing approach for deformable assemblies by extending the MIC with an explicit Coulomb frictional contact formulation. The formulation preserves the computational efficiency of MIC while capturing tangential interface mechanics governing stick and slip behavior in overconstrained assemblies.

The industrial case study demonstrated that incorporating friction significantly alters predicted interface forces and reduces tangential slip compared with frictionless NRVS assumptions. These results confirm that friction plays a critical role in geometry assurance for deformable assemblies and should be explicitly considered in tolerance analysis workflows. The proposed formulation enables scalable evaluation of frictional contact effects within digital twin environments for fixture design, locator layout, and joining strategy optimization. The current validation focuses primarily on force level comparison; future work will extend the approach to more advanced friction laws of interface behavior, e.g., pressure dependent friction and micro slip, and will address geometric validation using controlled experimental measurements.

Declaration of competing interest

The authors declare that they have no known competing financial interests or personal relationships that could have appeared to influence the work reported in this paper.

CRediT authorship contribution statement

Roham Sadeghi Tabar: Writing – review & editing, Writing – original draft, Visualization, Validation, Software, Resources, Project administration, Methodology, Investigation, Funding acquisition, Formal analysis, Data curation, Conceptualization. **Kristina Wärmefjord:** Writing – review & editing, Project administration, Methodology, Funding acquisition, Data curation. **Lars Lindkvist:** Validation, Software, Methodology, Investigation. **Rikard Söderberg (1):** Writing – review & editing, Software, Resources, Funding acquisition.

Acknowledgement

This work was conducted at Chalmers Wingquist Laboratory, AoA Production and supported by the Swedish Innovation Agency (Grant No 2024-02505). The support is gratefully acknowledged.

References

[1] Moroni G, Petrò S, Tolio T (2011) Early Cost Estimation for Tolerance Verification. *CIRP Annals* 60(1):195–198.
[2] Wang Y, Li L, Hartman N-W, Sutherland J-W (2019) Allocation of Assembly Tolerances to Minimize Costs. *CIRP Annals* 68(1):13–16.
[3] Söderberg R, Wärmefjord K, Carlson J-S, Lindkvist L (2017) Toward a Digital Twin for Real-Time Geometry Assurance in Individualized Production. *CIRP Annals* 66 (1):137–140.
[4] Franciosa P, Sokolov M, Sinha S, Sun T, Ceglarek D (2020) Deep Learning Enhanced Digital Twin for Closed-Loop In-Process Quality Improvement. *CIRP Annals* 69(1):369–372.
[5] Schleich B, Anwer N, Mathieu L, Wartzack S (2017) Shaping the Digital Twin for Design and Production Engineering. *CIRP Annals* 66(1):141–144.
[6] Lanza G, Haefner B, Kraemer A (2015) Optimization of Selective Assembly and Adaptive Manufacturing by Means of Cyber-Physical System Based Matching. *CIRP Annals* 64(1):399–402.
[7] Sadeghi Tabar R, Söderberg R, Ceglarek D, Franciosa P, Lindkvist L (2025) Augmented Geometry Assurance Digital Twin With Physics-Based Incremental Learning. *CIRP Annals* 74(1):151–155.
[8] Dantan J-Y, Eifler T (2021) Tolerance Allocation Under Behavioural Simulation Uncertainty of a Multiphysical System. *CIRP Annals* 70(1):127–130.
[9] Tabar R-S, Lorin S, Lindkvist L, Wärmefjord K, Söderberg R (2024) Robust Contact Computation in Non-Rigid Variation Simulation. *Journal of Manufacturing Science and Engineering* 24(8):081006.
[10] Morse E, Dantan J-Y, Anwer N, Söderberg R, Moroni G, Qureshi A, Jiang X, Mathieu L (2018) Tolerancing: Managing Uncertainty From Conceptual Design to Final Product. *CIRP Annals* 67(2):695–717.
[11] Wärmefjord K, Lindkvist L, Söderberg R, Lindau B, Andrén M (2023) Evaluation of Geometric Tolerances Using Strain Energy Density. *CIRP Annals* 72(1):109–112.
[12] Liu S-C, Hu S-J (1997) Variation Simulation for Deformable Sheet Metal Assemblies Using Finite Element Methods. *Journal of Manufacturing Science and Engineering* 119(3):368–374.
[13] Sadeghi Tabar R, Wärmefjord K, Söderberg R, Lindkvist L (2021) Critical Joint Identification for Efficient Sequencing. *Journal of Intelligent Manufacturing* 32:769–780.
[14] Homri L, Mirafzal M-R, Dantan J-Y (2023) A New Tolerance Allocation Approach Based on Decision Tree And Monte Carlo Simulation. *CIRP Annals* 72(1):105–108.
[15] Maltauro M, Meneghello R, Concheri G (2025) Enhancing Tolerance Stack-Up Analysis With Variable-Dependent Admissible Limits. *CIRP Annals* 74(1):157–160.
[16] Anwer N, Schleich B, Mathieu L, Wartzack S (2014) From Solid Modelling to Skin Model Shapes: Shifting Paradigms in Computer-Aided Tolerancing. *CIRP Annals* 63(1):137–140.
[17] Schleich B, Qie Y, Wartzack S, Anwer N (2022) Generative Adversarial Networks for Tolerance Analysis. *CIRP Annals* 71(1):133–136.
[18] Yan X, Ballu A (2018) Tolerance Analysis Using Skin Model Shapes and Linear Complementarity Conditions. *Journal of Manufacturing Systems* 48:140–156.
[19] Lorin S, Cromvik C, Edelvik F, Söderberg R (2015) Welding Simulation of Non-Nominal Structures With Clamps. *Journal of Computing and Information Science in Engineering* 15(2):21004.
[20] Lindau B, Wärmefjord K, Lindkvist L, Söderberg R (2013) Aspects of Fixture Clamp Modeling in Non-Rigid Variation Simulation of Sheet Metal Assemblies. In: *Proceedings of the ASME 2013 International Mechanical Engineering Congress and Exposition. Volume 2B: Advanced Manufacturing*, ASME, November 15–21, V02BT02A040.
[21] RD&T Technology AB (2017) RD&T Software Manual Mölndal, Sweden.